Molecular Crystals and Liquid Crystals Science and Technology. Section A. Molecular Crystals and Liquid Crystals

Publication details, including instructions for authors and subscription information:
http://www.tandfonline.com/loi/gmcl19

Computer Simulations of Nematic Defects

Axel Kilian [a]

[a] Institut für Theoretische Physik Technische Universität Berlin, D-1000, Berlin 12

Version of record first published: 04 Oct 2006.

To cite this article: Axel Kilian (1992): Computer Simulations of Nematic Defects, Molecular Crystals and Liquid Crystals Science and Technology. Section A. Molecular Crystals and Liquid Crystals, 222:1, 57-69

To link to this article: http://dx.doi.org/10.1080/15421409208048680

Mol. Cryst. Liq. Cryst. 1992, Vol. 222, pp. 57–69
Reprints available directly from the publisher
Photocopying permitted by license only

Printed in the United States of America

Computer Simulations of Nematic Defects

Axel Kilian
Institut für Theoretische Physik
Technische Universität Berlin
D-1000 Berlin 12

(Received September 30, 1991)

Abstract

The dynamics of nematic defects may not seem to be too important for device applications, if one knows how to avoid them. This may change in future, when disclinations can be used to store and process information, which appears possible due to their high entropy. The application of the differential equations of nemato-dynamics is however interesting from a theoretical point of view: it elucidates the capabilities and also the weaknesses of the present theory.

The numerical algorithm used here [1] is based on a dynamic equation for the alignment tensor $a_{\mu\nu}$, which takes the rotational diffusion, the influence of an orienting external field, and the Frank elasticity (in the one-coefficient approximation) into account. Flow processes are neglected.

First, I simulate the relaxation of randomly generated disclinations. The results are in accord with general topological laws [2] and with experimental observations. They demonstrate that disclination movement can occur as a pure reorientation process, without material flow. Second, the interesting behavior of disclinations subjected to an external field is investigated. It is found that the typical transient loops that occur during relaxation after a shear flow can be stopped from shrinking (and even caused to grow again) by an external electric field. I have confirmed this latter result by experiment [3]. As a more practical application of the numerical algorithm, the alignment and the relaxation of nematic droplets of spherical and ellipsoidal shape is simulated with different anchoring conditions at the boundary. The results may be helpful for modeling of the new PDLC (Polymer Dispersed Liquid Crystal) devices [4, 5].

1.0 History of the Nematic Defects

As early as 1904, O. Lehmann published this sketch [6]. It indicates that he already knew about the nematic symmetry and the topological shape of nematic defects, which he deduced from his numerous observations of liquid crystals under the polarization microscope.

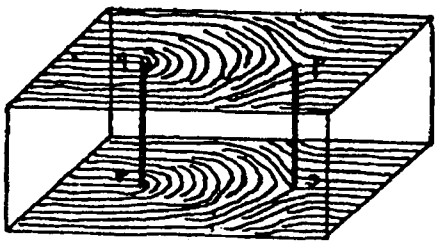

FIG.1 Hand sketch of disclination lines by O. Lehmann

He named the specific types of defects displayed here **half core points** and **half convergence points**, that is **disclinations of strength $\pm 1/2$** in today's notation.

In Fig.2, a typical Schlieren Texture is shown. Disclinations with half integer strength (2 brushes) as well as disclinations with integer strength (4 brushes) can occur.

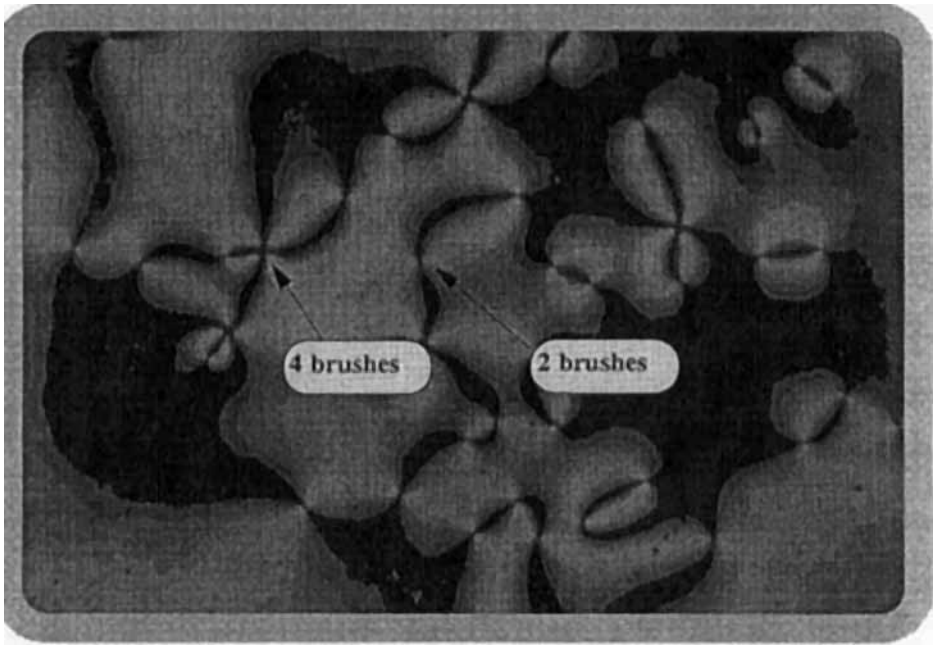

FIG.2 Typical nematic Schlieren texture viewed under crossed polarizers (by courtesy of K. Praefke, TU Berlin)

A quantitative model, which should explain the above features, was given by Oseen in 1933 [7]. It is based on isotropic first-order elasticity (later called Frank elasticity in the one-coefficient approximation). The free energy (per volume) is

$$f_d = \frac{K}{2} (\nabla \boldsymbol{n})^2 , \qquad \textit{(EQ 1)}$$

and for the director field $\boldsymbol{n}$, the ansatz

$$\boldsymbol{n} = \begin{pmatrix} \cos(u(\varphi)) \\ \sin(u(\varphi)) \\ 0 \end{pmatrix} \qquad \textit{(EQ 2)}$$

is chosen, where u is the polar angle in a spherical coordinate system parametrizing the director, and φ is the polar angle in a cylindrical coordinate system parametrizing physical space. The solutions that minimize the elastic energy are

$$u(\varphi) = s(\varphi - \varphi_o) . \qquad \textit{(EQ 3)}$$

The disclination strength s is half integer, and φ_0 any real number. Three examples are presented in Fig. 3, where it is understood that the extension in the third direction is homogeneous.

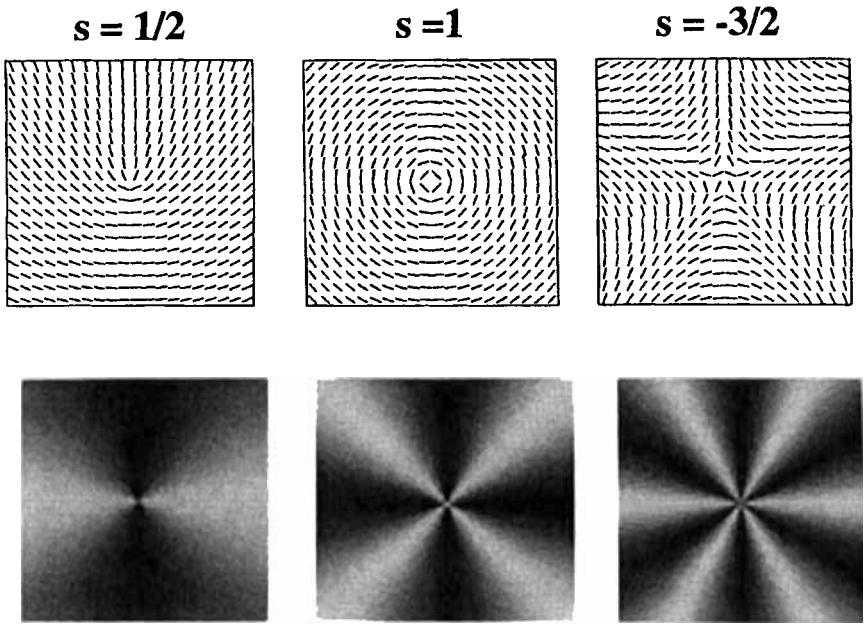

FIG.3 Three examples of the Oseen solution and the corresponding pictures as if viewed under crossed polarizers

Although both of the first two examples seem to meet the observed Schlieren textures (see Fig.2), we know today that the solutions with |s| = 1 are not stable, but rather an artifact of a constraint implied by the ansatz (2), as was found by R. B. Meyer [8] in 1973.

2.0 Theory

The orientation of (effectively) uniaxial molecules with their figure axis parallel to the unit vector **u** is characterized by the (second rank) alignment tensor

$$a_{\mu\nu} = \langle \overline{u_\mu u_\nu} \rangle \qquad (EQ\ 4)$$

The bracket <...> indicates an average (to be evaluated with the one-particle distribution function), and the bar refers to the symmetric-traceless (irreducible) part of the tensor. I assume the following nonlinear relaxation equation for **a** [9]:

$$\tau_a \frac{\partial a_{\mu\nu}}{\partial t} + \xi_o^2 \nabla^2 a_{\mu\nu} + \Phi_{\mu\nu}(\boldsymbol{a}) - F_{\mu\nu}(\boldsymbol{a}) = 0 \qquad (EQ\ 5)$$

The first term is a damping term; the second term describes the Frank elasticity in the one-coefficient approximation, i.e. $K_1 = K_2 = K_3$. The quantity $\Phi_{\mu\nu}$ is a generalized force represented by the derivatives of a (dimensionless) Landau-De Gennes potential, and $F_{\mu\nu}$ describes the influence of an external orienting field. The phenomenological coefficient ξ_0 is related to the Frank elastic constant according to

$$K = 3a_{eq}^2 \xi_0^2 \frac{\rho}{m} k_B T \qquad (EQ\ 6)$$

Further details may be looked up in [1]. This equation allows a unified treatment of non-equilibrium phenomena in the isotropic and the nematic phases, including the pretransitional phenomena. In view of the present purpose, which is to examine the general behavior of disclinations in the nematic phase, Eq. (5) can be simplified considerably by replacing the Landau-de Gennes term $\Phi_{\mu\nu}$ by the following two constraints:

a) uniaxiality, i.e. $a_{\mu\nu} = a\sqrt{\frac{3}{2}}\overline{n_\mu n_\nu}$.

b) $a = a_{eq} = S\sqrt{5}$, where $S = \langle P_2 (n_\mu u_\mu) \rangle$ is the Maier-Saupe order parameter.

The first condition is justified by the experimental fact, that thermotropic nematics (with few exceptions, cf. [10]) usually exhibit a uniaxial alignment, and by a recently performed linear stability analysis of the Landau-De Gennes potential, which revealed that the uniaxial state is stable [11].

Condition b), as will be shown, holds for any macroscopic length scale. It can be imposed by an exterior product, i.e.

$$\varepsilon_{\lambda\kappa\mu} a_{\kappa\nu} \left(\tau_a \frac{\partial a_{\mu\nu}}{\partial t} - \xi_o^2 \nabla a_{\mu\nu} - F_{\mu\nu} \right) = 0 \quad . \qquad (EQ\ 7)$$

where $\varepsilon_{\lambda\kappa\mu}$ is the totally antisymmetric tensor of rank 3.

3.0 The Numerical Algorithm

3.1 Simple form:

Equation (7) is discretized on a uniform mesh, and thereafter, condition b) is used. This results in the following numerical algorithm for a **constant scalar order parameter**:

$$n_\mu^{new} = \lambda \left[(\overline{n_\mu n_\nu} + \beta \hat{E}_\mu \hat{E}_\nu)\, n_\nu \right] \qquad (EQ\ 8)$$

The parameter λ has to be calculated at every lattice point such that $n_\mu n_\mu = 1$; γ_1 is the rotational viscosity, δl the mesh size, and K the Frank elastic constant. The maximum numerically-stable time step $\delta t = \gamma_1 \delta l^2/(6K)$ was chosen. The field strength E determines $\beta = \varepsilon_o \varepsilon_a \delta l^2 E^2/(6K)$.

The algorithm (8) has been used throughout this paper, with only one exception, namely when the influence of constraint b) was tested.

3.2 Extended form:

In principle, the scalar order parameter is not determined by the Landau-De Gennes potential alone, but also by the elastic interaction with the nematic environment, which is represented by the Laplacian in Eq. (5). In order to check the validity of the above assumption $a = a_{eq}$, I developed an extended numerical algorithm where the alignment is

still uniaxial, but the scalar order parameter a is free. This lead to the expression of an "alignment vector" $N_\mu = a\, n_\mu$. Its dynamics is given by

$$\tau_a \left(\frac{\partial}{\partial t} N_\mu - \frac{1}{3}\dot{a} n_\mu\right) - \xi_o^2 n_\nu \Delta\left(N_\mu n_\nu\right)$$

$$+ \left(A\left(T\right) - a + a^2\right) N_\mu - a^{-1} F_{\mu\nu} n_\nu = 0 \qquad \textit{(EQ 9)}$$

In order to get rid of meaningless parameters, all quantities in this equation are now scaled in units of combinations of B and C, the temperature-independent coefficients of the Landau-De Gennes potential. They should be distinguished from the previously defined quantities by a suitable tag, which I sacrifice for brevity.

The remaining parameter A(T) controls the temperature. Setting it to zero corresponds to T=T*, which is sometimes called the pseudo-critical temperature (below T*, no metastable isotropic phase is possible); the clearing point is at $A_c = 2/9$, and above $A^+ = 1/4$, the isotropic phase is stable, i.e. no metastable nematic phase is possible.

Discretizing Eq. (9) leads to the following numerical algorithm for the alignment vector:

$$N_\mu^{new} = \left(1 - \frac{\delta t}{\tau_a}\left(A - a + a^2\right)\right) N_\mu$$

$$+ \frac{\delta t}{\tau_a} \frac{\xi_o^2}{\delta x^2} \sum_{i=1}^{6} \left(N_\mu^i s^i - \left(\frac{2}{3} + \frac{a^i}{3a}\right) N_\mu\right) + a^{-1} F_{\mu\nu} n_\nu \qquad \textit{(EQ 10)}$$

Again, δx and δt are the mesh size and the time step, respectively.

3.3 Defect representation:

Due to the huge amount of data, it is not possible to represent the entire simulated director field. A sample is taken, which is done by selecting the sites with the highest anisotropic energy. In this way, the presentation resembles those pictures usually seen under the polarization microscope, because the locations with high anisotropic energy yield at the same time a high phase contrast for polarized light. It will be referred to as "defect representation". The defect representation shows only the vicinity of the disclinations and therefore enables the examination of the disclination type.

3.4 Periodic Boundary Conditions:

In principle, a simulated object does not require more space than its actual size. On the other hand, it is not desirable to restrict the orientational dynamics by physical boundaries other than the glass plates. The second condition interferes with the limited data storage of the computer. But it can be well approached by the method of periodic boundary conditions, which means identification of opposite boundaries. In this way, an infinite number of mirror images is generated. The simulated object exists in a finite but endless world.

4.0 Computer Simulations

General: the simulations presented here were performed on a mesh with 50 grid points in each dimension. I found this to be the minimum resolution to reproduce the complicated structure of disclination lines.

4.1 Variable scalar order parameter

The scalar order parameter a takes usually its equilibrium value, a_{eq}. This, however, does not hold in the vicinity of disclinations, nor in the core. Wondering, what advantages (if any) a "smooth" solution with a variable scalar order parameter would yield, I applied the extended numerical algorithm to a disclination.

Setup: as an initial state, a disclination of the Oseen type with s=1/2 was modelled. Rigid boundary conditions were applied, and a temperature of $T = T^*$ was chosen. In order to obtain a visibly decreasing order parameter in the computer simulation, a length scaling (spatial resolution of the simulation) of $\xi_0/\delta x = 6$ was applied.

Result: Fig. 4 exhibits the equilibrium configuration. The length of the director symbol reflects the value of a. In most known substances, ξ_0 is a material parameter of the order of a molecular length. For example, in MBBA $\xi_0 = 1.2$ nm, see Eq. (6), and the molecular length is 2.5 nm.

The scalar order parameter varies within one molecular length between its equilibrium value and zero.

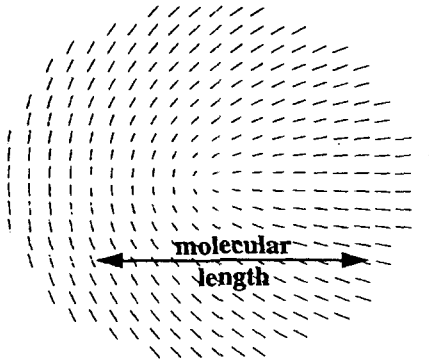

FIG.4 The scalar order parameter (the length of the alignment vector) is diminished inside a disclination core

Discussion: the extended algorithm behaves as it should, i.e., it simulates correctly the decrease of the scalar order parameter caused by a strong curvature of the director field. Qualitatively, this is known from experiment, e.g. the light scattering at the isotropic core of thin disclination lines, and the recently examined surface melting [12]. The additional quantitative information provided by the extended algorithm is, how exactly the order parameter decreases.

Besides the fact that statements of that kind (quite sophisticated solutions have been presented previously, [13-15]) can hardly be verified or falsified by experiment, they even appear doubtful within the framework of the underlying continuum theory.

4.2 Relaxation from the isotropic state

General: from now on, the simpler algorithm with a constant scalar order parameter is applied.

Setup: the initial state consists of isotropically distributed random vectors. Rigid, parallel boundary conditions were applied.

Result: The relaxation process proceeds from total disorder via a network of disclination lines (a so-called Frank network) to a shrinking loop that finally vanishes. Fig. 5 exhibits nine stages.

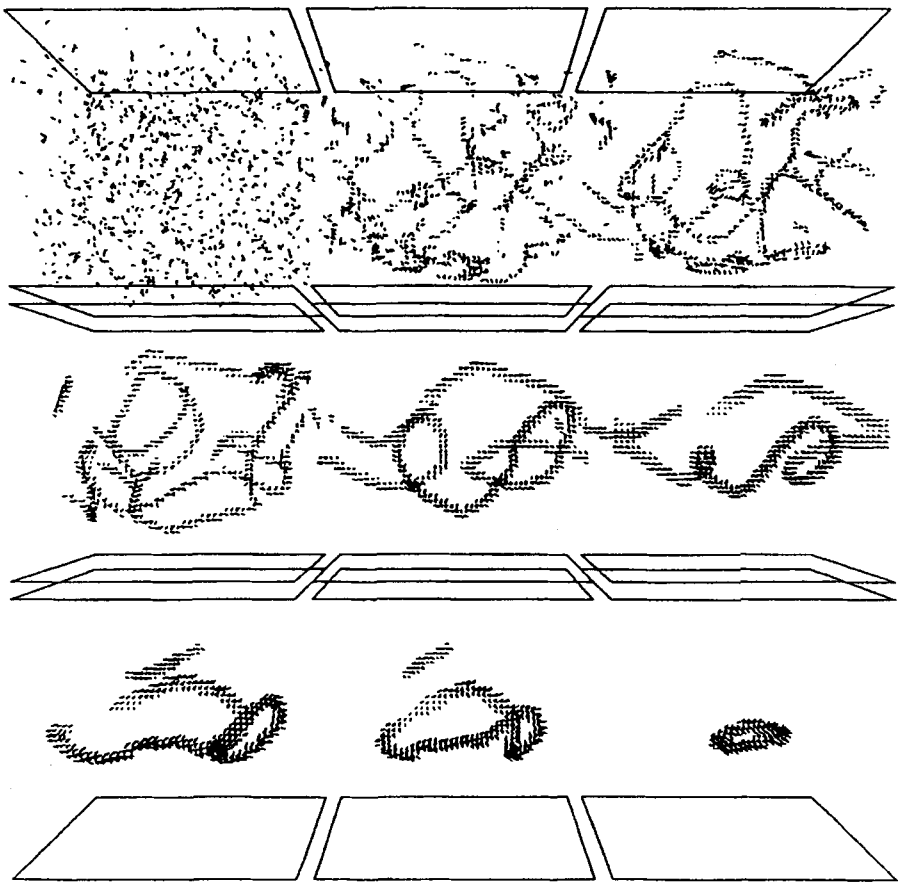

FIG.5 Relaxation from a quasi-isotropic state. The director configuration proceeds via a Frank network and a shrinking loop to total order (the last state is not shown here)

Discussion: this simulation is interesting from several points of view:

1. It shows, in accord with experiment, that defects occur usually as lines.
2. It shows that the impression of a moving pattern does not imply a material flow; an orientation transport is sufficient.
3. It supports the group-theoretical result that only endless disclination lines can be topologically stable, which is demonstrated here by a (transient) closed loop.

One of the powers of computer simulation is the random access to all physical quantities. Whereas the experimentalist could only observe a shrinking loop, the simulation reveals the topological shape of the director field:

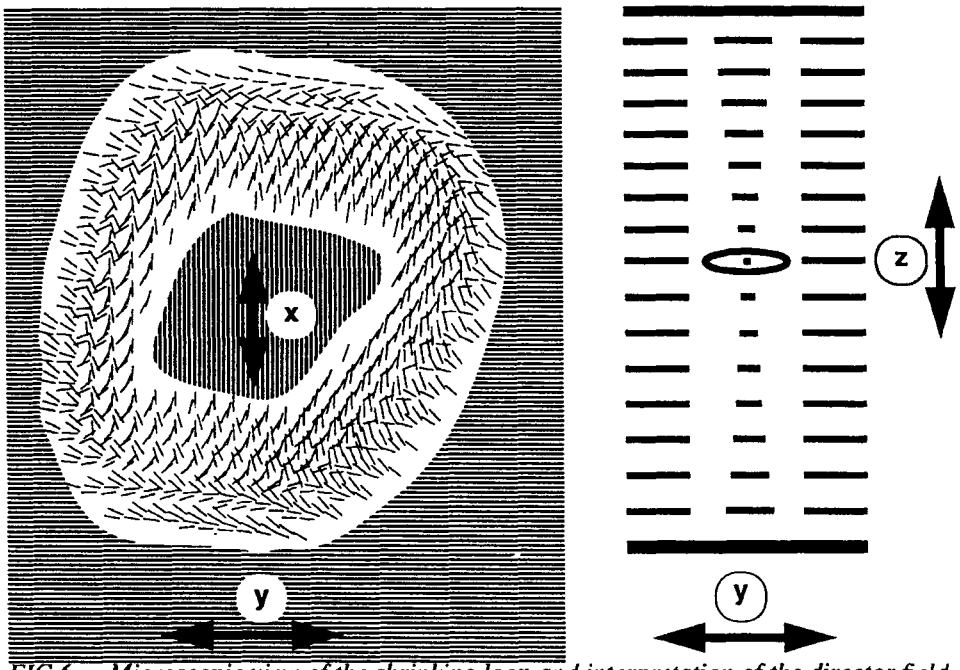

FIG.6 Microscopic view of the shrinking loop and interpretation of the director field

The loop is the border line between a 180° twist region (the interior) and a homogeneously aligned region (the rest).

This scenario is equivalent to a reverse twist disclination, where the boundary conditions are also planar, but mutually perpendicular.

4.3 Escape into the 3. Dimension?

This simulation is somewhat artificial; I did it mainly to confront the numerical algorithm with an impossible object, or, to put it another way, to check wether the algorithm is consistent with R. B. Meyer's paper [8] "On the existence of even-indexed disclination lines".

An endless s=1 disclination can be continuously transformed into a defect-free dome-structure (escape into the 3. dimension). But is it likely that this happens spontaneously?

Setup: the initial state is a modelled s=1 disclination line of the Oseen type, which was fixed at the boundaries (rigid anchoring).

Result: The disclination line does not transform into a defect free dome-structure, but splits into two lines of strength 1/2. Fig. 7 shows a cross section through the splitting line. It supports the group-theoretical conservation law of the topological charges, i.e. the disclination winding number. Fig. 8 gives a three-dimensional view on the splitting line at six stages of the relaxation process

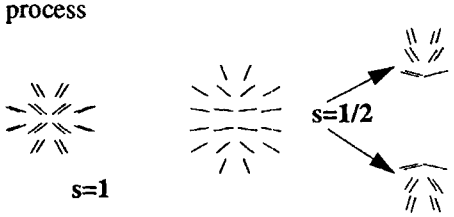

FIG.7 A cross section through the splitting s=1 disclination line at three subsequent times.

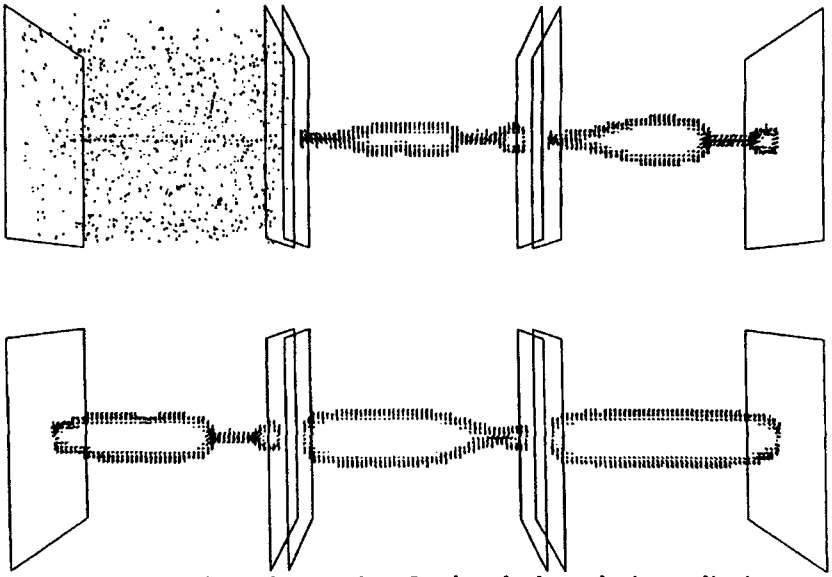

FIG.8 A disclination line of strength 1, fixed at the boundaries, splits into two lines of strength 1/2. This indicates a repelling force between equally charged defects.

4.4 Electric Field effects

Setup: the data from the shrinking loop simulation 4.2 at a time just before the loop vanished were taken as the initial state, and an increasing electric field (in direction perpendicular to the boundaries) was applied, assuming a positive dielectric anisotropy.

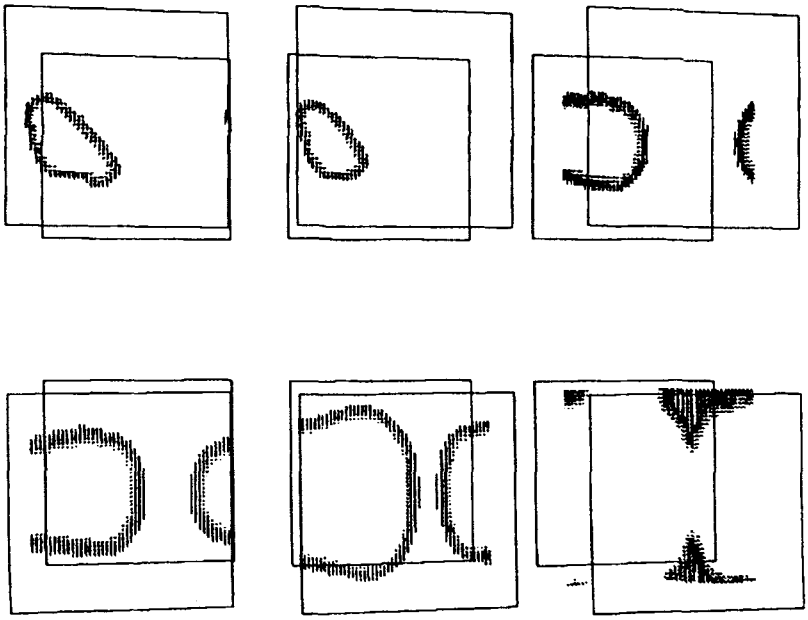

FIG.9 Upon applying an external electric field, a disclination loop stops shrinking and grows until it collides with its mirror images (which were generated by periodic boundary conditions)

Discussion: in the light of the above described director configuration, it appears plausible that an external field would first orient the interior of the loop, due to the lower Fredericks threshold in the present case of a twisted director configuration. Accordingly, this area switches similar to a twist cell, whereas the area outside does not switch simultaneously (the Fredericks threshold is higher), but rather does the loop grow in size.

I confirmed this prediction experimentally. For details see [3].

4.5 Nematic Droplets

Presently, a new generation of devices -the PDLCD and PDCLCD - Polymer Dispersed (Cholesteric) Liquid Crystal Device [4, 5] is being developed. For them to operate, the presence of disclinations is essential.

I simulated nematic droplets of spherical and ellipsoidal shape, with planar and homeotropic surface alignment. Homeotropic anchoring can be assumed rigid (boundary conditions of the first kind), whereas in the planar case, there is no preferred direction for the alignment. Consequently, the director field at the surface is then allowed to rotate freely within the local tangent plane.

This new kind of boundary conditions (which, by the way, would be hard to handle analytically) led to an interesting result of more general significance: it provides a microscopic model for the s=1 surface disclinations, which does not require any additional assumptions.

Planar alignment: a basic theorem in differential geometry says that there is no global section of the tangent bundle of a sphere. This means that for the droplet with planar anchoring, the director field at the surface cannot be defect-free. It is known from experiment [4], that for comparable K_1 and K_3 the droplets exhibit a so called polar configuration. This configuration possesses two antipodal s=1 point-disclinations at the surface, which define the droplet axis. The overall alignment coincides fairly well with this axis.

Experiments have shown that the equilibrium orientation of the polar axis is governed by two influences:

1. the cavity form, i.e. the deviation from the spherical shape, and
2. an external field.

The orientation of the axis by an external orienting field worked fine. Unfortunately, I was not able to reconfirm the first result. An anisotropic cavity could not induce a preferred direction for the polar axis. This may have two reasons:

1. Either, it is the one-coefficient approximation, which is not sensitive for an anisotropic distribution of bend-splay distortions, or
2. the reorientation by cavity anisotropy is coupled with a flow process.

The graphical representation of the simulated droplets includes three features: the cavity shape, the director field in the defect representation (the disclinations) and the over-all alignment, i.e. the averaged alignment tensor. Although the alignment is locally uniaxial by constraint, the mean alignment may become biaxial. The symbol for the mean alignment is a rectangular box, which is built with the eigenvectors and eigenvalues of $n_\mu n_\nu$. It is a cube for isotropic alignment, and a square cylinder for uniaxial alignment. The averaging corresponds to a low spatial resolution in experiment, or to very small droplets.

Fig. 10 shows the relaxation of the director field of a spherical droplet from an isotropic state.

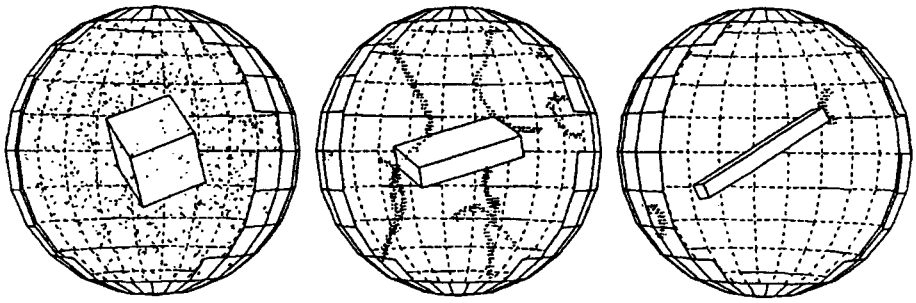

FIG.10 Three stages of the relaxation of a nematic droplet from the isotropic state. A network of disclination lines simplifies to two short antipodal half-loops.

During the relaxation, in non-equilibrium, a transient biaxiality occurs. The equilibrium configuration exhibits a strong polar axis. At the poles, short half-loops of s=1/2 disclination lines have established. They are topologically equivalent to s=1 points (compare Fig. 7). The axis is randomly oriented.

Next, the axis is oriented parallel to the cavity z-axis by an external field, assuming a positive dielectric anisotropy. This process is not shown here, I just mention that the disclinations move to the poles, and again, a transient biaxiality occurs.

Fig. 11a shows a photograph of a nematic droplet viewed along the polar axis with a polarizing microscope, which was recently taken by Doane et al. [4]. Fig. 11b is a contrast picture calculated from the above simulation. It is simply the square of the averaged component a_{xy} of the alignment tensor, corresponding to polarizers in x- and y-direction, respectively. In Fig. 11c, the droplet in the defect representation is shown.

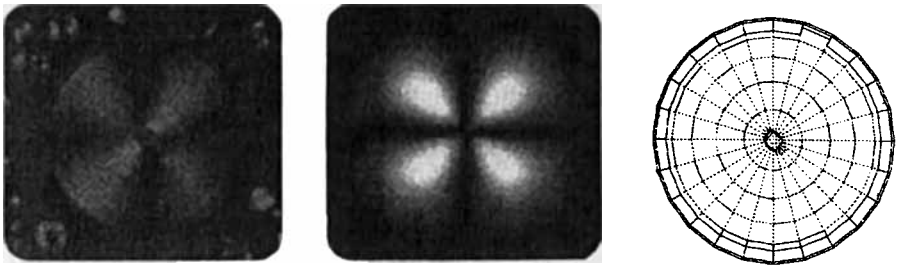

Polarizing microscope photograph **(Doane et al.1991)**

Density plot of $(\overline{n_x n_y})^2$ of the simulated droplet

Defect view of the simulated droplet

FIG.11 Bipolar configured nematic droplet viewed along the polar axis.

Discussion: The polar configuration is correctly reproduced. The reorientation of the cavity axis, however, cannot be explained by the simple model. The optical model, although simple, is sufficient to reproduce the typical textures viewed under the polarizing microscope.

Homeotropic alignment: the computer simulation yields, in accord with experiment, an equilibrium configuration characterized by a hedgehog disclination point in the center of

the droplet. The overall orientation is fairly isotropic, and can be aligned by an external field.

In the planar case the s=1 surface disclinations were realized by short half-loops. Similarly, the hedgehog point here is realized by a small ring in the center. The environment of the ring, of course, is topologically identical to that of a hedgehog point, as can be deduced from the overall orientation, which is isotropic in either case.

5.0 Conclusions and Acknowledgments

The numerical method proved capable to simulate the complicated structures of the nematic defects. The relaxation from the quasi-isotropic state illustrates that the impression of a moving pattern does not necessarily imply a material flow.

On the base of the correct nematic symmetry and a new type of boundary conditions, i.e. true planar anchoring, a "microscopic" explanation of the s=1 surface disclination points arose without any additional assumptions.

A new electric field effect was predicted with the aid of the numerical algorithm and confirmed experimentally. This demonstrates the reliability of the method.

An enhancement of the algorithm including a variable scalar order parameter failed to bring in any additional information that could be considered relevant; the simple model, which is essentially a director theory with the correct head-tail symmetry appears sufficient to describe the disclinations examined here. I am, however, convinced that there are physical situations where a variable scalar order parameter plays an essential role, e.g. in the blue phases.

The simplicity of the method (no flow, equal elastic constants) may be considered as a weakness; I see it as an advantage: it allows one to judge which physical mechanisms are essential for a particular effect. So far, it illustrates the variety of effects based solely on orientation transport and isotropic first-order elasticity. The failure of the reorientation of bipolar configured droplets by cavity anisotropy, therefore, is a first success: only a stepwise enhancement of the numerical procedure will help to recognize the relevant physical mechanisms. The extension to three elastic constants, and to cholesteric substances, is in progress.

Financial support of the Deutsche Forschungsgemeinschaft via the Sonderforschungsbereich "Anisotrope Fluide" is gratefully acknowledged. I thank Prof. Dr. S. Hess and Dr. F. Oestreicher (TU Berlin) for their assistance.

6.0 References

[1] A. Kilian and S. Hess, Z. Naturforsch. **44a**, 693 (1989);
Liq. Cryst. **8**, 465 (1990)

[2] M. Kleman, *Points, Lines and Walls*, J. Wiley & Sons, New York (1983)

[3] A. Kilian, Mol. Cryst. Liq. Cryst. Lett. **8** (5), 91 (1992)

[4] J. W. Doane, A. Golemme, J. L. West, J. B. Whitehead and B. G. Wu, Mol. Cryst. Liq. Cryst. **165**, 511 (1988);
Renate Ondris-Crawford, Evan P. Boyko, Bryan G. Wagner, John H. Erdmann, Slobodan Zumer, and J. William Doane, J. App. Phys. **69** (9), 6380 (1991)

[5] P. P. Crooker and D. K. Yang, Appl. Phys. Lett. **57**, 2529 (1990)

[6] O. Lehmann, *Die Lehre der flüssigen Kristalle und ihre Beziehung zu den Problemen der Biologie* (Bergmann, Wiesbaden, 1917)

[7] C. W. Oseen, Trans. Faraday Soc. **29**, 883 (1933)

[8] R. B. Meyer, Phil. Mag. **27**, 405 (1973)

[9] S. Hess and I. Pardowitz, Z. Naturforsch. **36a**, 554 (1981)

[10] K. Praefke, B. Kohne, B. Gündogan, D. Singer, D. Demus, S. Diele, G. Pelzl, and U. Bakowsky, Mol. Cryst. Liq. Cryst. **198**, 393 (1991)

[11] P. Kaiser and S. Hess, J. Nonequilib. Thermodyn., accepted for publication (1991)

[12] G. Barbero and G. Durand, J. App. Phys. **69** (10), 6968 (1991)

[13] E. C. Gartland, Jr., P. Palffy-Muhoray and R. S. Varga, Mol. Cryst. Liq. Cryst. **199**, 429 (1991)

[14] C. Fan, Phys. Lett. **34a**, 335 (1971)

[15] N. Schohpohl and T. J. Sluckin, Phys. Rev. Lett. **59**, 2589, (1987)